SCIENCE CHINA
Physics, Mechanics & Astronomy

• Article •
Progress of Projects Supported by NSFC

May 2014 Vol.57 No.5: 844–848
doi: 10.1007/s11433-014-5419-z

Proton angular distribution research by a new angle-resolved proton energy spectrometer

SU LuNing[1], ZHENG Yi[1], LIU Meng[1], HU ZhiDan[1], WANG WeiMin[1], YUAN XiaoHui[2], XU MiaoHua[3], SHENG ZhengMing[1,2], SHEN ZhongWei[1], FAN HaiTao[1], LI YuTong[1*], MA JingLong[1], LU Xin[1], CHEN LiMing[1], WANG ZhaoHua[1], WEI ZhiYi[1] & ZHANG Jie[1,2*]

[1] *Beijing National Laboratory for Condensed Matter Physics, Institute of Physics, Chinese Academy of Sciences, Beijing 100190, China;*
[2] *Key Laboratory for Laser Plasmas (MoE) and Department of Physics, Shanghai Jiao Tong University, Shanghai 200240, China;*
[3] *Department of Physics, China University of Mining and Technology (Beijing), Beijing 100083, China*

Received January 23, 2014; accepted February 12, 2014; published online March 13, 2014

The proton spectral and angular distributions simultaneously within the target normal direction and laser propagation direction by using an angle-resolved proton energy spectrometer are studied. For the protons generated in the interactions of 100 fs, 800 nm laser pulses with aluminum foil targets, the deviations of proton beam centers of different energies from the target normal direction towards the laser propagation direction are different. This is probably because of the toroidal magnetic fields generated at the rear target surface, which deflect protons transversely. As a result, protons in low energy range have large deviation angles, protons in middle energy range have the smallest deviation angles, while protons in high energy tail have large deviation angles.

laser-driven, proton, acceleration

PACS number(s): 52.38.Kd, 52.50.Jm, 41.75.Jv

Citation: Su L N, Zheng Y, Liu M, et al. Proton angular distribution research by a new angle-resolved proton energy spectrometer. Sci China-Phys Mech Astron, 2014, 57: 844–848, doi: 10.1007/s11433-014-5419-z

1 Introduction

Laser-driven proton acceleration has been studied for decades. Because of the advantages in short pulse duration, high brightness and small source size, the proton beams have many potential applications in proton radiography [1], proton-driven fast ignition in the inertial confinement fusion [2], medical therapy [3] and proton-driven nuclear reactions [4]. To obtain proton beams with good qualities, many aspects of proton acceleration have been studied, such as proton spectra [5], acceleration mechanisms and proton angular distributions. In most experiments of laser-driven-accelerated protons, the nuclear track detector CR-39 stacks and the medical dose detector radiochromic film (RCF) stacks are usually used to detect proton angular distributions. By using CR-39 and RCF stacks, Zepf et al. [6] studied the angular distribution of laser-driven accelerated protons; three proton sources were found in the laser-solid interactions. Using CR-39 stacks, Lindau et al. [7] investigated the deviation of the accelerated protons towards the laser propagation (LP) direction in target normal sheath acceleration (TNSA) mechanism. Fuchs et al. [8] used RCF stacks to detect proton distribution, in order to find the difference of electron propagation in conductor and insulator in the proton acceleration. Because of the Bragg peak, protons at different layers of CR-39 or RCF stacks correspond to different proton energies. Proton spectra in different directions

*Corresponding author (LI YuTong, email: ytli@aphy.iphy.ac.cn; ZHANG Jie, email: jzhang@aphy.iphy.ac.cn)

could be estimated roughly by the combination of the data of several layers of CR-39 or RCF. However, the energy resolution is not good. Comprehensive and accurate measurements of proton beams are important to understand protons generation, control and applications.

Here, using a new angle-resolved proton energy spectrometer, which can detect proton angular distributions and energy spectral information simultaneously [9], we have studied proton spectra and angular distributions within target normal (TN) direction and LP direction. We find that proton beam centers deviate from the TN direction towards the LP direction. Proton count peaks at different energies have different emitting angles.

2 Experimental setup

The experiment was performed on the Xtreme Light (XL) III Ti: sapphire laser system at the Institute of Physics, Chinese Academy of Sciences [10]. The XL-III laser system employed chirp pulse amplification (CPA) technology. The laser pulse duration was approximately 100 fs, the central wave length was 800 nm in the experiment. The experimental setup schematic is shown in Figure 1. A p-polarized laser pulse was focused by an f/1.67 off-axis parabola (OAP) mirror onto the solid target foil obliquely at an incidence angle of 15°. The full width at half maximum (FWHM) of the laser focal spot was 8 μm. The contrast ratio at nanoseconds before the arrival of the main laser pulse was better than 10^{-6}. With the laser pulse energies of 1–2.5 J, the laser intensity could reach 1.5×10^{19} W cm^{-2} in the experiment. The targets were 1.2 μm and 2.5 μm thick aluminum foils.

An angle-resolved proton energy spectrometer [9], which was set at 8 cm away from the target, was used to detect proton spectra within the LP direction and the TN direction. Instead of a pinhole typically used in a traditional Thomson parabolic spectrometer, a horizontal lead pinhole array which contained 16 pinholes was used as the entrance of the angle-resolved spectrometer. The distance of the two proximal pinhole centers was 1.5 mm, and the diameter of each pinhole was 0.5 mm. A slowly varying magnetic field with central field strength of 0.3 T was applied in the spectrometer. We used 98 mm×49 mm imaging plates (IP) behind the spectrometer to detect protons. As a result of the Gaussian distribution of the magnetic field, protons with same energy passing through different pinholes would have different deflection distances on the imaging plate. We calculated the proton spectra using the calibration data in each pinhole. A 12.5 μm thick aluminum filter was used to cover the IP, in order to block carbon ions with energies of less than 14 MeV. In our experiment, we did not observe carbon ions and other ions with energies of higher than 4 MeV by using a traditional Thomson parabolic spectrometer. As a result, only protons with energies of higher than 0.9 MeV were detected by the IP.

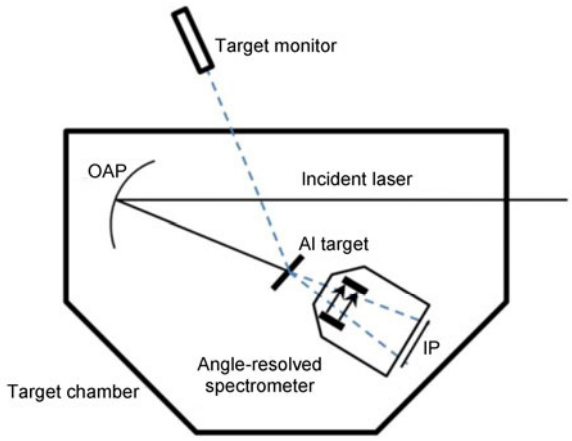

Figure 1 Schematic view of experimental setup. Laser pulse that was p-polarized was focused by an f/1.67 OAP mirror onto the aluminum foil obliquely at an incidence angle of 15°. FWHM of the laser focal spot was 8 μm, and the maximum laser intensity was 1.5×10^{19} W cm^{-2}. Target monitor was used to adjust the target position. Horizontal lead 16-pinhole array in front of the angle-resolved spectrometer was used to collect protons within the LP direction and the TN direction.

3 Results and discussions

In the angle-resolved spectrometer, the horizontal magnetic field can deflect protons passing different pinholes separately, forming 16 proton traces on the IP, as shown in Figure 2. The marked positions above are the signals from neutral particles and photons, corresponding to the original entrances. The vertical ordinate corresponds to energy dispersion, while the horizontal ordinate corresponds to angular distribution. The collection angle of the angle-resolved spectrometer is 16°. Therefore, we could obtain accurate proton spectra within 16° in our experiment simultaneously.

Figure 2 shows the raw proton image on the imaging plate behind the angle-resolved spectrometer from the interactions of 1.6 J laser pulse and 1.2 μm Al foil target. Because the 12.5 μm aluminum filter before the imaging

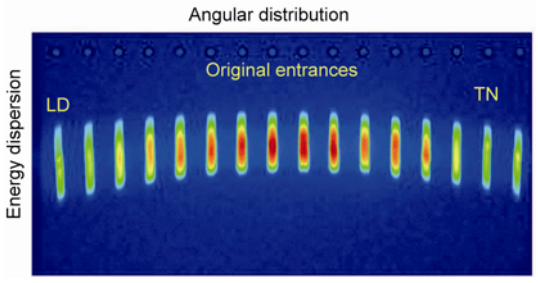

Figure 2 Raw proton image on the imaging plate. Marked 16 rounds are the original entrances. Horizontal ordinate corresponds to the angular distribution, and the vertical ordinate corresponds to energy dispersion. First line from the left corresponds to the proton spectrum in the LP direction, while the second line from the right to the proton spectrum in the TN direction.

plate blocked the protons with energies < 0.9 MeV, there were no signals in the lower part. The second line from the right corresponds to the TN direction, while the first line from the left to the LP direction. The angle of the TN direction is set to be 0°. The angle of the LP direction is 15°. We plot the proton spectra in the TN direction and the LP direction as shown in Figure 3, the proton counts are given per 1 MeV and per 1 sr. The two spectra almost follow the exponetial-like distribution, and the high energy sections (3.2–4.0 MeV) are almost the same. However, there is some differences in the low and middle energy sections (0.9–3.0 MeV).

We have used different thick targets in experiment. For 1.2 μm and 2.5 μm thick targets, we plot the proton maximum energy and energy-integrated proton count versus emitting angle in Figures 4(a) and (b), respectively. The proton maximum energy and proton count of the 1.2 μm target are much higher than those of the 2.5 μm target. For 2.5 μm Al target, the center of proton beam is 1.1° to the TN direction, which is smaller than that of 1.2 μm Al target.

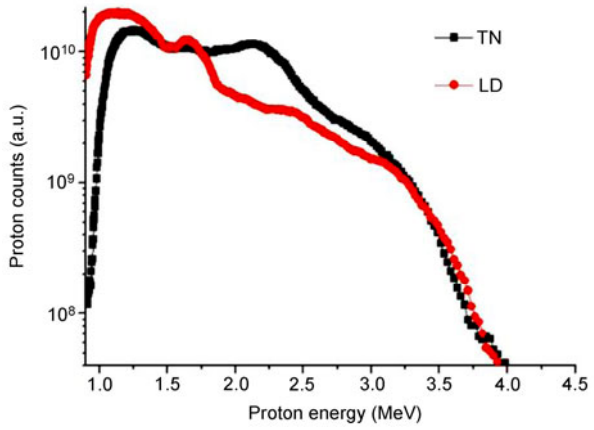

Figure 3 Proton spectra in the TN direction and the LP direction. Two spectra are similar in high energy section above 3.2 MeV, and different in low and middle energy sections. Both spectra almost follow the exponential-like distribution, and have some modulations in the middle energy section.

These deviations of the proton beam center from the TN direction towards the LP direction are probably caused by the pre-plasma expansion before the arrival of the laser pulse [11]. The amplification of spontaneous emission (ASE) of the laser could generate shock waves in the target front. The shock waves propagate to and modify the target rear surface, making a pre-plasma expansion at the target rear surface. As a result, the actual TN directions are changed by the shock waves. For thinner targets, shock waves will arrive at the target rear surface earlier, making a larger pre-plasma expansion. Therefore, the deviation of the proton beam for the thinner targets is larger than that for the thicker targets.

For 1.2 μm Al target, the angular distributions of proton maximum energy and energy-integrated proton count both obey Gaussian distribution. However, their peaks are in different directions. For proton maximum energy, the peak is at 5.3° to the TN direction; while for energy-integrated proton count, the peak is at 7.5° to the TN direction. This difference should be the result of the different angular distributions of protons with different energies.

We plot proton counts with 8 different energy sections versus emitting angle as shown in Figure 5. Proton counts with lower energies are more than those with higher energies, while protons with higher energy are more collimated. Interestingly, the peaks of the 8 lines in Figure 5 correspond to different angles, which indicates that the centers of proton beams in different energy sections are in different directions. A polynomial fitting has been taken for each line to estimate the center of the proton beam for each energy section. We plot the angle of proton count peaks versus proton energy section as shown in Figure 6. For the protons of 1.0–2.0 MeV, the deviations of proton count peaks are the largest at approximately 6.9°. They become smaller with proton energy increasing to 3.0–3.5 MeV, where they are the smallest at about 3.3°. When proton energy increases from 3.5 MeV to 5.0 MeV, the deviations rise from 3.3° to 5.3°. This result is similar to the suggestion given by Sheng et al. [12]. However, the deviations in each energy section

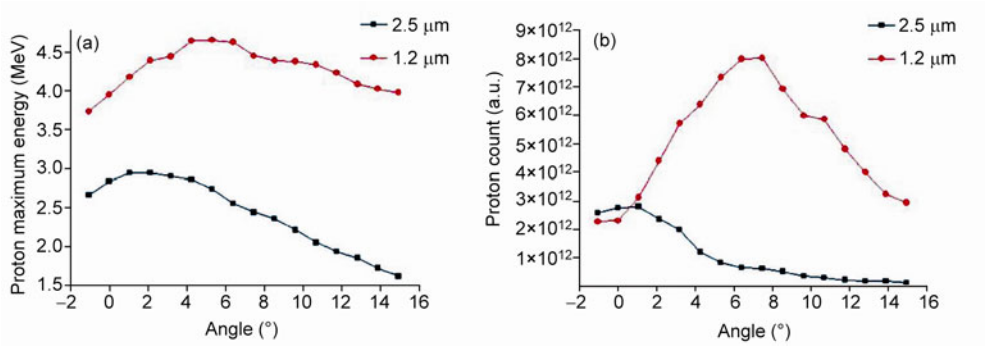

Figure 4 (a) Proton maximum energy versus proton emitting angle. (b) Energy-integrated proton counts versus proton emitting angle. Black square line corresponds to 2.5 μm Al target, while the red round line to 1.2 μm Al target. Two angular distributions follow the Gaussian distribution. Peaks of the two distributions are at different angles.

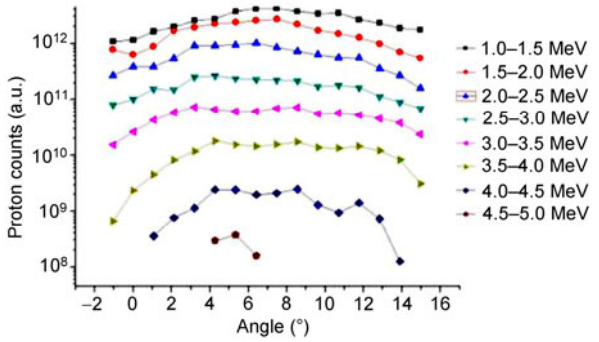

Figure 5 Proton counts with 8 different energy sections versus emitting angle. Eight energy sections are separated by 0.5 MeV. Proton counts in lower energy sections are more than those in higher energy sections. Peaks of different line correspond to different angles.

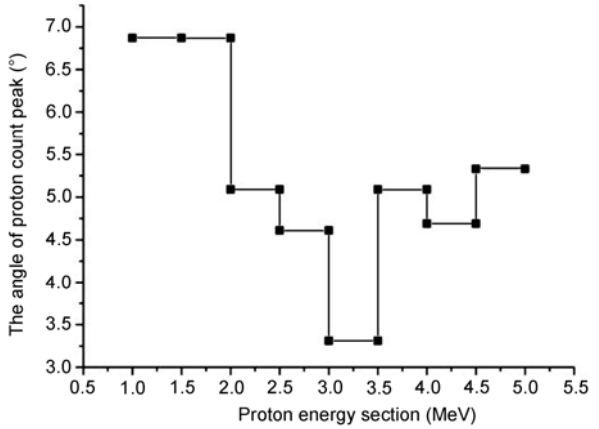

Figure 6 Angle of proton count peaks versus proton energy section. For the protons of 1.0–2.0 MeV, the deviations of proton count peaks are the largest at about 6.9°. They become smaller with proton energy increasing to 3.0–3.5 MeV, where they are the smallest at about 3.3°. When proton energy increases from 3.5 MeV to 5.0 MeV, the deviations rise from 3.3° to 5.3°.

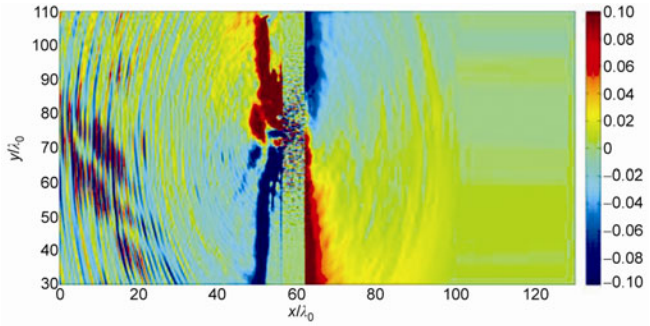

Figure 7 Distribution of the self-generated magnetic fields in the PIC simulations. Magnetic field strength is up to 10 MGauss.

in the suggestion given by Sheng et al. [12] are much smaller than that in our experiment. The individual particle model is used to estimate proton angular distribution, and the pre-plasma expansion at the target rear surface is not concerned in the work by Sheng et al. [12].

By proton radiography, Sarri et al. [13] has shown that there are self-generated toroidal magnetic fields in the target rear surface during the interactions of ultra-short laser and solid foils. We believe that the self-generated magnetic fields deflect the accelerated protons, forming the different deviations of protons with different energies. To confirm this, we carry out 2D3V particle in cell simulations with the code KLAPS [14,15]. The simulation region is $40\lambda_0 \leqslant x \leqslant 50\lambda_0$, $-35\lambda_0 \leqslant y \leqslant 35\lambda_0$, where λ_0 and τ_0 are laser wavelength and laser period, respectively. The temporal and spatial resolutions in the simulations are $\mathrm{d}t=0.025\,\tau_0$, and $\mathrm{d}x=\mathrm{d}y=0.025\lambda_0$. For both electrons and protons, 36 simulation particles are put in each cell. Similar to our experiment, a Gaussian laser beam with a normalized vector potential a=2.4 is incident from the left boundary at an angle of 15°. The target has a uniform density of $30n_c$, where n_c is the plasma critical density. The pre-plasma density scale-length is set to be $2\lambda_0$. We plot the magnetic fields in the simulations as shown in Figure 7. The magnetic field strength is up to 10 MGauss. Protons with lower energy are deflected more by the magnetic fields than those with higher energy. As a result, the protons in the low energy sections have more deviations. For the high sections, protons have a long accelerating time by the TN sheath electric field; they also have a long period affected by the self-generated magnetic field. Hence, protons in high energy sections have large deflection angles. For the middle energy section, protons neither have a long accelerating time, nor are affected most by the magnetic fields; therefore, they have the smallest deflection angles. However, the influences of the magnetic field on the accelerated protons are complex. Further studies are needed to fully understand the role of the magnetic field.

4 Conclusions

By a new angle-resolved proton energy spectrometer, we have studied proton angular distributions within the TN direction and the LP direction. The results show that the angular distributions of proton maximum energy and proton counts in small energy sections follow the Gaussian distribution. However, proton count peaks in different energy sections are in different angles, probably because of the effect of the self-generated toroidal magnetic fields in the target rear surface. Proton count peaks in low energy sections have large deviation angles, those in middle energy sections have small deviation angles, while those in high energy sections have large deviation angles as well.

This work was supported by the National Basic Research Program of China (Grant No. 2013CBA01501) and the National Natural Science Foundation of China (Grant Nos. 11375262 and 11135012).

1 Borghesi M, Campbell D H, Schiavi A, et al. Electric field detection in laser-plasma interaction experiments via the proton imaging technique. Phys Plasmas, 2002, 9: 2214–2220
2 Roth M, Cowan T E, Key M H, et al. Fast ignition by intense laser-accelerated proton beams. Phys Rev Lett, 2001, 86: 436–439
3 Bulanov S V, Khoroshkov V S. Feasibility of using laser ion accelerators in proton therapy. Plasma Phys Rep, 2002, 28: 453–456
4 Ledingham K W D, McKenna P, Singhal R P. Applications for nuclear phenomena generated by ultra-intense lasers. Science, 2003, 300: 1107–1111
5 Cui Y Q, Wang W M, Sheng Z M, et al. Quasimonoenergetic proton bunches generation from doped foil targets irradiated by intense lasers. Phys Plasmas, 2013, 20: 024502
6 Zepf M, Clark E L, Beg F N, et al. Proton acceleration from high-intensity laser interactions with thin foil targets. Phys Rev Lett, 2003, 90: 064801
7 Lindau F, Lundh O, Persson A, et al. Laser-accelerated protons with energy-dependent beam direction. Phys Rev Lett, 2005, 95: 175002
8 Fuchs J, Cowan T E, Audebert P, et al. Spatial uniformity of laser-accelerated ultrahigh-current MeV electron propagation in metals and insulators. Phys Rev Lett, 2003, 91: 255002
9 Zheng Y, Su L N, Liu M, et al. A new angle-resolved proton energy spectrometer. Rev Sci Instrum, 2013, 84: 096103
10 Wang Z H, Liu C, Shen Z W, et al. High-contrast 1.16 PW Ti:sapphire laser system combined with a doubled chirped-pulse amplification scheme and a femtosecond optical-parametric amplifier. Opt Lett, 2011, 36: 3194–3196
11 Xu M H, Li Y T, Yuan X H, et al. Effects of shock waves on spatial distribution of proton beams in ultrashort laser-foil interactions. Phys Plasmas, 2006, 12: 104507
12 Sheng Z M, Sentoku Y, Mima K, et al. Angular distributions of fast electrons, ions, and bremsstrahlung X/γ-rays in intense laser interaction with solid targets. Phys Rev Lett, 2000, 85: 5340–5343
13 Sarri G, Macchi A, Cecchetti C A, et al. Dynamics of self-generated, large amplitude magnetic fields following high-intensity laser matter interaction. Phys Rev Lett, 2012, 109: 205002
14 Wang W M, Sheng Z M, Norreys P A, et al. Electron energy deposition to the fusion target core for fast ignition. J Phys-Conf Ser, 2010, 244: 022070
15 Chen M, Sheng Z M, Zheng J, et al. Developments and applications of multi-dimensional particle-in-cell codes in the investigation of laser plasma interactions. Chin J Comput Phys, 2008, 25: 43–50